

Article

Novel Waveform Design with a Reduced Cyclic Prefix in MIMO Systems

Huanhuan Yin ¹, Jiehao Luo ^{2,*}, Baobing Wang ³, Bing Zhang ², Shuang Luo ² and Dejin Kong ² 

¹ The Beidou Academy, Wuhan Qingchuan University, Wuhan 430000, China; hhyin155@126.com

² School of Electronic and Electrical Engineering, Wuhan Textile University, Wuhan 430000, China; 2215363027@mail.wtu.edu.cn (B.Z.); 2215363008@mail.wtu.edu.cn (S.L.); djkou@wtu.edu.cn (D.K.)

³ Anhui Fengsung Electronics Co., Ltd., Tongling 244000, China; wang.baobing@tong-feng.com

* Correspondence: 2215363047@mail.wtu.edu.cn

Abstract: For well-known orthogonal frequency division multiplexing (OFDM), the cyclic prefix (CP) is essential for coping with multipath channels. Nevertheless, CP is a pure redundant signal, which wastes valuable time–frequency resources. We propose a novel waveform based on symbol repetition, which is presented to cut down the CP overhead in OFDM. In the presented OFDM with symbol repetition (SR-OFDM), one CP is inserted in the front of several transmitted symbols, instead of only one symbol, as in the conventional way. As a result, it can save the overhead created by CP. Furthermore, due to the existence of the remaining CP, the multipath channel can still be converted into the frequency domain, and single-tap equalization can still be used to equalize information free from interference. In addition, we also extend the proposed SR-OFDM into multiple input–multiple output (MIMO) systems. Finally, the proposed schemes are validated by computer simulations under the various channels.

Keywords: cyclic prefix (CP); orthogonal frequency division multiplexing (OFDM); multipath channel; single-tap equalization; multiple input–multiple output (MIMO)



Citation: Yin, H.; Luo, J.; Wang, B.; Zhang, B.; Luo, S.; Kong, D. Novel Waveform Design with a Reduced Cyclic Prefix in MIMO Systems. *Electronics* **2024**, *13*, 1968. <https://doi.org/10.3390/electronics13101968>

Academic Editor: Adão Silva

Received: 9 April 2024

Revised: 10 May 2024

Accepted: 14 May 2024

Published: 17 May 2024



Copyright: © 2024 by the authors. Licensee MDPI, Basel, Switzerland. This article is an open access article distributed under the terms and conditions of the Creative Commons Attribution (CC BY) license (<https://creativecommons.org/licenses/by/4.0/>).

1. Introduction

The cyclic prefix (CP) technique has become well known for its remarkable resistance to the multipath effect, and has been employed in various modulations [1,2], especially orthogonal frequency division multiplexing (OFDM). OFDM divides the available spectrum into multiple orthogonal subcarriers, each carrying a portion of the data. This parallel transmission scheme enables efficient spectrum utilization and high data rates. Furthermore, OFDM employs a cyclic prefix (CP) to guard against channel delay spread, simplifying equalization at the receiver. In essence, CP involves the insertion of a known segment of data at the beginning of each OFDM symbol, which is identical to the symbol's ending segment. This technique effectively extends the time domain of the transmitted signal, allowing for better resistance against multipath interference at the receiver. The receiver will demodulate and equalize the samples in the data symbol interval to recover the information affected by the channel, while the samples in the CP interval will be discarded. By removing the cyclic prefix at the receiver, the overlapping signals caused by multipath propagation can be effectively mitigated, thereby improving the overall reliability and performance of the communication system. However, CP is also considered to be a purely redundant signal that wastes a lot of valuable time–frequency resources [3]. For example, the CP overheads in 4G are 7% and 25% for normal-CP frame and extended-CP frame, respectively. Moreover, in scenarios where the channel conditions are relatively stable, the use of CP may be perceived as unnecessary, as the benefits of combating multipath interference are not fully realized. As a consequence, the reduction of CP without causing interference or distortion plays a vital role in improving spectral efficiency and has attracted much attention.

Currently, many attempts have been made to successfully reduce CP in OFDM. Since the CP is related to the channel impulse response (CIR), reducing the CP overhead can be achieved by shortening the CIR. In [4], a scheme to shorten the CIR utilizing a time domain equalizer (TEQ) is proposed. The TEQ is cascaded with the channel to maximize the CIR energy within a given window, thereby reducing the effective CIR and minimizing the CP. In [5], the authors attempted to directly shorten the CP of the transmitted signal, and to cope with the accompanying interference, a sum-rate optimization was applied, and then a precoding matrix was acquired. This precoding matrix performs interference suppression by eliminating frequency-valued zeros within the frequency-selective channel band without knowledge of channel state information (CSI). In [6], the authors proposed a joint optimization algorithm based on the Peak-to-Mean Envelope Power Ratio (PMEPR) and Peak-to-Sidelobe Level Ratio (PSLR) to address interference issues during clipping and frequency domain filtering processes. This approach aims to reduce CP while maintaining high-speed transmission. In [7], the Residual Intercoder Interference Cancellation (RISIC) algorithm is proposed, which cancels inter-symbol interference (ISI) by performing CP reconfiguration and tail cancellation at the receiver. Ref. [8] proposes a simple strategy for serial interference cancellation and parallel interference cancellation to address the insufficient CP-induced inter-carrier interference and ISI. However, parallel interference cancellation entails higher hardware complexity, while serial interference cancellation requires larger detection delays. Since interference cancellation considers interference from all subcarriers, the computational burden becomes significant when the subcarrier number is large. In addition, scholars have proposed CP-free OFDM systems. In [9], a symbol cyclic shift equalization (SCSE) algorithm is introduced to reduce the CP overhead in OFDM systems by utilizing a stored feedback equalizer. SCSE utilizes decision feedback equalization (DFE) before demodulation to eliminate any interference between overlapping OFDM symbols, effectively transforming linear convolution into circular convolution and enabling FFT-based demodulation of the received signal at the receiver. SCSE requires repeated FFT/IFFT operations, leading to a high level of computational complexity. In [10], a successive multipath interference cancellation (SMIC) algorithm is proposed for CP-free OFDM systems, leveraging stored feedback equalization (SFE) to mitigate ISI. The SMIC algorithm offers lower computational complexity and a considerably shorter feedback loop compared to DFE methods. Ref. [11] proposes a hybrid prefix (HP) OFDM, which reduces the average length of the prefix by employing a low-complexity detector to recover the effective signal. However, HP-OFDM achieves short prefixes at the expense of performance loss and increased complexity. Despite attempts to reduce the CP, interference arises directly from the shortened CP of the OFDM signal [12]. Dealing with this interference typically requires algorithms of high complexity. Nevertheless, residual interference persists and significantly affects symbol demodulation, particularly under high signal-to-noise ratio (SNR) conditions.

We propose a novel waveform based on symbol repetition to cut down the CP overhead in OFDM. In the presented OFDM with symbol repetition (SR-OFDM), one CP is inserted in the front of several transmitted symbols, rather than inserting CP in front of each symbol, as is the case in classic OFDM. As a result, the number of CPs in SR-OFDM can be greatly reduced. To maintain the data rate, multiple symbols can be designed and transmitted simultaneously in an orthogonal manner through multiple branches. Furthermore, due to the existence of the one remaining CP, the multipath channel can still be converted into the frequency domain, and single-tap equalization can still be used to equalize information free from the multipath effect.

The remainder of this paper is composed as follows. In Section 2, we provide a detailed description of the proposed SR-OFDM system, including how to design the signal, single-tap equalization, and demodulation of the received signal. In addition, we extend the proposed SR-OFDM into multiple input–multiple output (MIMO) systems to improve the spectral efficiency in Section 3. Finally, in Section 4, the proposed schemes are validated by simulations.

2. Proposed Low CP Waveform

In this section, a novel waveform based on symbol repetition is presented to reduce the CP overhead. While it is indispensable for preserving signal integrity amidst channel distortions, the inclusion of CP preceding each symbol introduces a considerable overhead, depleting precious bandwidth and diminishing the spectral efficiency. In the proposed scheme, one symbol occupies Y symbol durations, i.e., the symbol is repeated Y times. During the Y symbol durations, no CP is inserted, which is different from the classical OFDM. Meanwhile, $Y - 1$ other symbols are designed and transmitted simultaneously by $Y - 1$ branches in an orthogonal manner, which guarantees that the data rate will not be reduced compared to classical OFDM. Finally, one CP is inserted in front of the Y symbol durations. It will be shown that, due to the existence of this one CP, the multipath channel can still be converted into the frequency domain, and single-tap equalization can still be used to equalize information that is free from multipath effects.

2.1. SR-OFDM Transmitter

Figure 1a shows the flowchart of the SR-OFDM transmitter, in which Y symbols are transmitted by Y branches simultaneously during Y symbol intervals. Suppose the number of subcarriers is N . For the v -th branch, transmitted symbols $d_{n,v}$ with subcarrier index $n \in [0, N - 1]$ and branch index $v \in [0, Y - 1]$, pass through a N -point inverse discrete Fourier transform (IDFT), and it is written as

$$s_v(k) = \frac{1}{\sqrt{N}} \sum_{n=0}^{N-1} d_{n,v} e^{j\frac{2\pi nk}{N}}, \quad k \in [0, N - 1]. \tag{1}$$

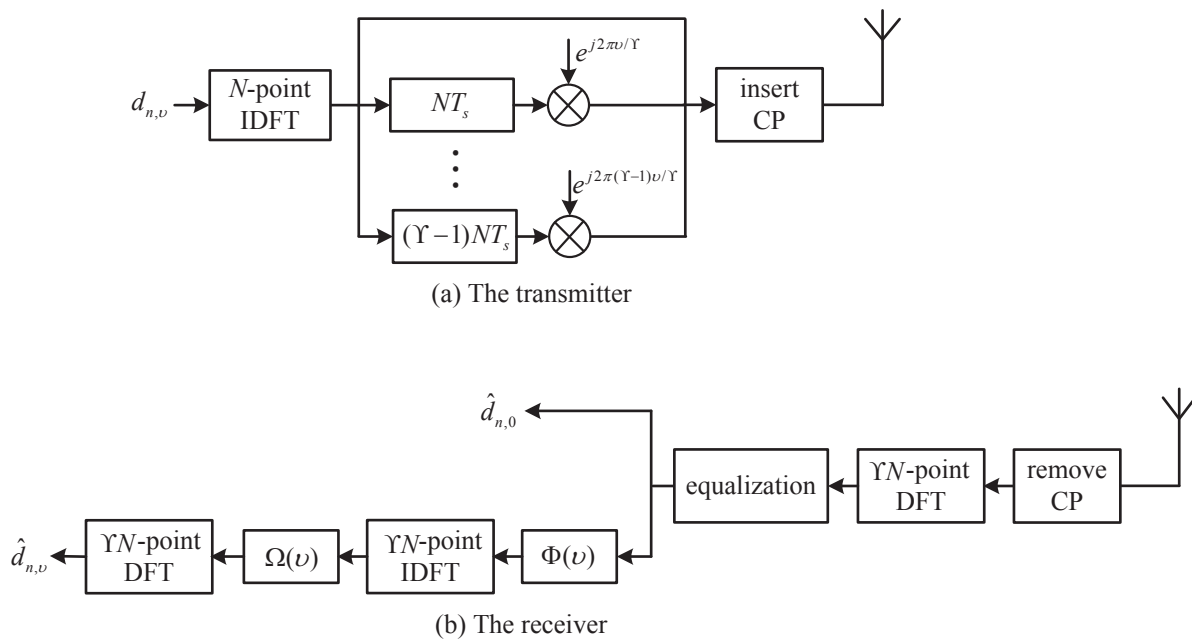


Figure 1. The system diagram of SR-OFDM.

Subsequently, $s_v(k)$ is transmitted repeatedly for Y times, and the signal can be written as

$$\begin{aligned} \bar{s}_v(k) &= s_v(k) e^{j\frac{2\pi v\alpha k}{Y}}, \quad k = \alpha N + \tilde{k}, \\ \alpha &\in [0, Y - 1] \quad \tilde{k} \in [0, N - 1]. \end{aligned} \tag{2}$$

The CP resists multi-path interference by replicating samples from the tail of the signal. Therefore, SR-OFDM replicates the tail samples of $\bar{s}_v(k)$ as the CP. When the signal is inserted into the CP, the signal is obtained

$$\tilde{s}_v(k) = \begin{cases} \bar{s}_v(YN + k), & k \in [-L_{cp}, -1], \\ \bar{s}_v(k), & k \in [0, YN - 1]. \end{cases} \quad (3)$$

where L_{cp} represents the CP length. When $k \in [-L_{cp}, -1]$, $\bar{s}_v(k)$ is considered to be the CP, $YN + k$ serves as an index for the tail sample.

Finally, the transmitted signal can be obtained as

$$\tilde{s}(k) = \sum_{v=0}^{Y-1} \tilde{s}_v(k). \quad (4)$$

The signal $\bar{s}_v(k)$ is inserted into the CP, and the signal is obtained $\tilde{s}_v(k)$. The transmitted signal consists of different branches, $\tilde{s}_v(k)$, denoted as $\tilde{s}(k)$. When $v = 2$, the structure of transmitted SR-OFDM with CP is shown in Figure 2.

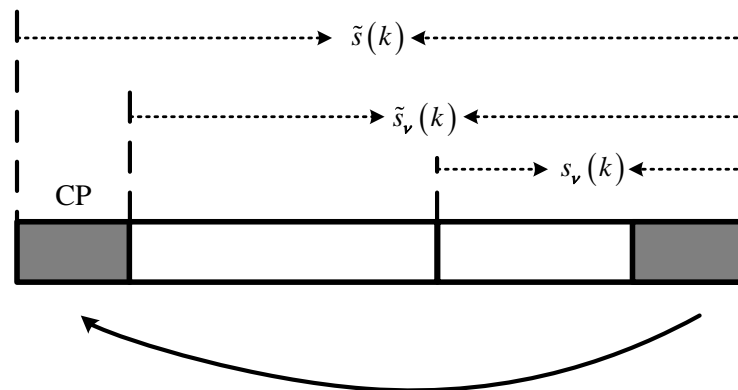


Figure 2. The transmitted SR-OFDM with CP, when $v = 2$.

The transmitted signal can be conveyed through various means, such as a single antenna or multiple antennas, laying the groundwork for integration with MIMO technology.

2.2. SR-OFDM Receiver

Denote the channel as $h(k)$ with the maximum path delay L_h [13–15]. The received signal can be obtained via the convolution between the transmitted signal $\tilde{s}(k)$ and the channel $h(k)$. Thus, it is written as

$$r(k) = \sum_{l=0}^{L_h-1} h(k-l)\tilde{s}(k) + \eta(k), \quad k \in [-L_{cp}, YN + L_h - 2]. \quad (5)$$

where $\eta(k)$ is additive white Gaussian noise (AWGN).

At the receiver in Figure 1b, after removing CP, the signal is expressed as

$$\tilde{r}(k) = \sum_{l=0}^{L_h-1} h(k-l)\tilde{s}(k) + \eta(k), \quad k \in [0, YN - 1]. \quad (6)$$

By performing a YN -point discrete Fourier transform (DFT) on $\tilde{r}(k)$, the signals for different v in $d_{n,v}$ can be separated, significantly reducing the complexity. Then, we can obtain

$$y_{\tilde{n}} = \frac{1}{\sqrt{YN}} \sum_{k=0}^{YN-1} \tilde{r}(k) e^{-\frac{j2\pi\tilde{n}k}{YN}}. \tag{7}$$

According to Equations (4) and (6), we have

$$\begin{aligned} y_{\tilde{n}} &= \frac{1}{\sqrt{YN}} \sum_{k=0}^{YN-1} \sum_{l=0}^{L_h-1} h(l) \tilde{s}(k-l) e^{-\frac{j2\pi\tilde{n}k}{YN}} + \eta_{\tilde{n}} \\ &= \frac{1}{\sqrt{YN}} \sum_{r=0}^{Y-1} \left[\sum_{l=0}^{L_h-1} h(l) e^{-\frac{j2\pi\tilde{n}l}{YN}} \right] \sum_{k=-l}^{YN-1-l} \tilde{s}_v(k) e^{-\frac{j2\pi\tilde{n}k}{YN}} + \eta_{\tilde{n}}, \end{aligned} \tag{8}$$

where $\tilde{n} \in [0, YN - 1]$. In addition, $\eta_{\tilde{n}}$ is written as

$$\eta_{\tilde{n}} = \frac{1}{\sqrt{YN}} \sum_{k=0}^{YN-1} \eta(k) e^{-\frac{j2\pi\tilde{n}k}{YN}}. \tag{9}$$

Note that the signal $\tilde{s}_v(k)$ has a circular structure; (8) is rewritten as

$$\begin{aligned} y_{\tilde{n}} &= \frac{1}{\sqrt{YN}} \sum_{v=0}^{Y-1} \left[\sum_{l=0}^{L_h-1} h(l) e^{-\frac{j2\pi\tilde{n}l}{YN}} \right] \\ &\quad \times \sum_{k=0}^{YN-1} \tilde{s}_v(k) e^{-\frac{j2\pi\tilde{n}k}{YN}} + \eta_{\tilde{n}}, \end{aligned} \tag{10}$$

For simplicity, denote $\sum_{l=0}^{L_h-1} h(l) e^{-j2\pi\tilde{n}l/YN}$ as $H_{\tilde{n}}$. Next, according to (2), $y_{\tilde{n}}$ can be rewritten as

$$\begin{aligned} y_{\tilde{n}} &= \frac{H_{\tilde{n}}}{\sqrt{YN}} \sum_{v=0}^{Y-1} \sum_{k=0}^{YN-1} \tilde{s}_v(k) e^{-\frac{j2\pi\tilde{n}k}{YN}} + \eta_{\tilde{n}} \\ &= \frac{H_{\tilde{n}}}{\sqrt{YN}} \sum_{v=0}^{Y-1} \sum_{k=0}^{YN-1} s_v(\tilde{k}) e^{\frac{j2\pi v\tilde{k}}{Y}} e^{-\frac{j2\pi\tilde{n}k}{YN}} + \eta_{\tilde{n}}, \end{aligned} \tag{11}$$

where $k = \alpha N + \tilde{k}$, $\tilde{k} \in [0, N - 1]$, and $\alpha \in [0, Y - 1]$. From Equation (1), it holds that

$$s_v(k) = s_v(\tilde{k}), \tag{12}$$

where $k = \alpha N + \tilde{k}$. As a result, we obtain

$$y_{\tilde{n}} = \frac{H_{\tilde{n}}}{N\sqrt{Y}} \sum_{v=0}^{Y-1} \sum_{k=0}^{YN-1} \sum_{n_0=0}^{N-1} d_{n_0,v} e^{\frac{j2\pi k(n_0 Y - \tilde{n} + v)}{YN}} e^{-\frac{j2\pi v\tilde{k}}{YN}} + \eta_{\tilde{n}}. \tag{13}$$

Define $\tilde{n} = nY + \alpha$, with $n \in [0, N - 1]$ and $\alpha \in [0, Y - 1]$. Next, (13) is expressed as

$$y_{nY+\alpha} = \frac{H_{nY+\alpha}}{N\sqrt{Y}} \sum_{v=0}^{Y-1} \sum_{k=0}^{YN-1} \sum_{n_0=0}^{N-1} d_{n_0,v} e^{\frac{j2\pi k(n_0 Y + v - nY - \alpha)}{YN}} e^{-\frac{j2\pi v\tilde{k}}{YN}} + \eta_{nY+\alpha}. \tag{14}$$

Kindly observe that the ensuing equations remain valid at all times,

$$\sum_{k=0}^{YN-1} e^{\frac{j2\pi k(n_0Y+v-nY-\alpha)}{YN}} e^{-\frac{j2\pi vk}{YN}} = \begin{cases} \varepsilon, & \text{if } \alpha = v, \\ 0, & \text{otherwise.} \end{cases} \quad (15)$$

Then, we can obtain

$$y_{nY+v} = \frac{H_{nY+v}}{N\sqrt{Y}} \sum_{n_0=0}^{N-1} d_{n_0,v} \sum_{k=0}^{YN-1} e^{\frac{j2\pi k(n_0-n)}{N}} e^{-\frac{j2\pi vk}{YN}} + \eta_{nY+v}. \quad (16)$$

According to (16), it can be easily observed that $y_{\tilde{n}}$, $\tilde{n} = nY + v$ hinges on the index v in $d_{n_0,v}$. That is to say, y_{nY+v_1} is only determined by d_{n_0,v_1} and y_{nY+v_2} is only determined by d_{n_0,v_2} . Therefore, d_{n_0,v_1} and d_{n_0,v_2} can be recovered independently due to the lack of overlap of the signal.

2.2.1. Symbol Recovery of $d_{n,0}$

For $v = 0$, y_{nY+v} is obtained

$$y_{nY} = \frac{H_{nY}}{N\sqrt{Y}} \sum_{n_0=0}^{N-1} d_{n_0,0} \sum_{k=0}^{YN-1} e^{\frac{j2\pi k(n_0-n)}{N}} + \eta_{nY}. \quad (17)$$

Due to the orthogonality of OFDM, i.e.,

$$\sum_{k=0}^{YN-1} e^{j2\pi k(n_0-n)/N} = \begin{cases} YN, & \text{if } n_0 = n, \\ 0, & \text{otherwise.} \end{cases} \quad (18)$$

The signal y_{nY} becomes

$$y_{nY} = \sqrt{Y}H_{nY}d_{n,0} + \eta_{nY}, \quad n = 0, 1, \dots, N - 1. \quad (19)$$

Then, a single-tap equalizer is performed to obtain $\hat{d}_{n,0}$, i.e.,

$$\hat{d}_{n,0} = \frac{y_{nY}}{\sqrt{Y}H_{nY}}, \quad n = 0, 1, \dots, N - 1. \quad (20)$$

The transmitted symbols $d_{n,v}(k)$ are demodulated at the receiver as $\hat{d}_{n,v}(k)$. From (20), the transmitted symbols $d_{n,0}$ are free from multipath effects.

2.2.2. Symbol Recovery of $d_{n,v}$, $v \in [1, Y - 1]$

For $v \neq 0$, the signal is

$$y_{nY+v} = \frac{H_{nY+v}}{N\sqrt{Y}} \sum_{n_0=0}^{N-1} d_{n_0,v} \sum_{k=0}^{YN-1} e^{\frac{j2\pi k(n_0-n)}{N}} e^{-\frac{j2\pi vk}{YN}} + \eta_{nY+v}. \quad (21)$$

When H_{nY} has been identified, the single-tap equalization can be conducted on y_{nY+v} , i.e.,

$$\begin{aligned} \tilde{y}_{nY+v} &= \frac{y_{nY+v}}{H_{nY+v}} \\ &= \frac{1}{N\sqrt{Y}} \sum_{n_0=0}^{N-1} d_{n_0,v} \sum_{k=0}^{YN-1} e^{\frac{j2\pi k(n_0-n)}{N}} e^{-\frac{j2\pi vk}{YN}} + \tilde{\eta}_{nY+v}, \end{aligned} \quad (22)$$

where $\tilde{\eta}_{nY+v} = \eta_{nY+v}/H_{nY+v}$. Equation (22) shows that \tilde{y}_{nY+v} only hinges on the $d_{n_0,v}$ with respect to the index v . Therefore, to recover the symbol $d_{n_0,v}$, the signal is obtained

$$\Gamma_{\tilde{n},v} = \Phi(v) = \begin{cases} \tilde{y}_{nY+v}, & \text{if } \tilde{n} = nY + v, \\ 0, & \text{otherwise.} \end{cases} \tag{23}$$

Then, after the IDFT operator, the signal is obtained

$$\begin{aligned} \tilde{\Gamma}_{m,v} &= \frac{1}{\sqrt{YN}} \sum_{\tilde{n}=0}^{YN-1} \Gamma_{\tilde{n},v} e^{\frac{j2\pi\tilde{n}m}{YN}} \\ &= \frac{1}{\sqrt{Y^2N^3}} \sum_{\tilde{n}=0}^{YN-1} \sum_{n_1=0}^{N-1} d_{n_1,v} \sum_{k=0}^{YN-1} e^{\frac{j2\pi k(n_1-n)}{N}} e^{-\frac{j2\pi v\tilde{k}}{YN}} e^{\frac{j2\pi\tilde{n}m}{YN}} + \hat{\eta}_{m,v}. \end{aligned} \tag{24}$$

Note that $\hat{\eta}_{m,v}$ is

$$\hat{\eta}_{m,v} = \frac{1}{\sqrt{YN}} \sum_{n=0}^{N-1} \tilde{\eta}_{nY+v} e^{-\frac{j2\pi(nY+v)m}{YN}}. \tag{25}$$

Define a phase coefficient, i.e.,

$$\Omega(v) = e^{-\frac{j2\pi vp}{Y}} = e^{-\frac{j2\pi v(m-\tilde{m})}{YN}}, \tag{26}$$

$$\begin{aligned} \Theta_{m,v} &= \frac{1}{\sqrt{Y^2N^3}} \sum_{\tilde{n}=0}^{YN-1} \sum_{n_1=0}^{N-1} d_{n_1,v} \sum_{k=0}^{YN-1} e^{\frac{j2\pi k(n_1-n)}{N}} e^{-\frac{j2\pi v\tilde{k}}{YN}} e^{\frac{j2\pi\tilde{n}m}{YN}} e^{-\frac{j2\pi vp}{Y}} + \hat{\eta}_{m,v} \\ &= \frac{1}{\sqrt{Y^2N^3}} \sum_{\tilde{n}=0}^{YN-1} \sum_{n_1=0}^{N-1} d_{n_1,v} \sum_{k=0}^{YN-1} e^{\frac{j2\pi k(n_1-n)}{N}} e^{-\frac{j2\pi v\tilde{k}}{YN}} e^{\frac{j2\pi\tilde{n}m}{YN}} e^{-\frac{j2\pi vpN}{YN}} + \hat{\eta}_{m,v}. \end{aligned} \tag{27}$$

$$\Theta_{m,v} = \frac{1}{\sqrt{Y^2N^3}} \sum_{n_1=0}^{N-1} d_{n_1,v} \sum_{k=0}^{YN-1} \sum_{\tilde{n}=0}^{YN-1} e^{-\frac{j2\pi(k-m)\tilde{n}}{YN}} e^{\frac{j2\pi kn_1Y}{YN}} e^{\frac{j2\pi vK}{YN}} e^{-\frac{j2\pi v\tilde{k}}{YN}} e^{-\frac{j2\pi vm}{YN}} e^{\frac{j2\pi v\tilde{m}}{YN}} + \hat{\eta}_{m,v}. \tag{28}$$

where $m = pN + \tilde{m}$, $\tilde{m} = 0, 1, \dots, N - 1$, and $p \in [0, Y - 1]$. Then, we can obtain $\Theta_{m,v} = \tilde{\Gamma}_{m,v}\Omega(v)$, which is depicted in (27). Also, let $pN = m - \tilde{m}$ with $m \in [0, YN - 1]$ and $\tilde{m} \in [0, N - 1]$, and (27) can be rewritten as (28). Subsequently, $\Theta_{m,v}$ is written as

$$\Theta_{m,v} = \frac{1}{\sqrt{N}} \sum_{n_1=0}^{N-1} d_{n_1,v} e^{\frac{j2\pi mn_1}{N}} + \hat{\eta}_{m,v}, \tag{29}$$

where $\tilde{n} = nR + v$, $v \in [1, Y - 1]$, $m = \alpha N + \tilde{m}$, $k = \alpha N + \tilde{k}$, and $\tilde{k} = 0, 1, \dots, N - 1$. In addition, $\hat{\eta}_{m,v} = \tilde{\eta}_{m,v}e^{-j2\pi v(m-\tilde{m})/YN}$. Equation (29) shows that, for the index v , there exists a repetition structure for $\Theta_{m,v}$.

After the DFT operator, symbol demodulation is obtained, i.e.,

$$\begin{aligned} \hat{\Theta}_{\tilde{n},v} &= \frac{1}{\sqrt{YN}} \sum_{m=0}^{YN-1} \Theta_{m,v} e^{-\frac{j2\pi m\tilde{n}}{YN}} \\ &= \frac{1}{\sqrt{YN^2}} \sum_{m=0}^{YN-1} \sum_{\tilde{n}=0}^{N-1} d_{n,v} e^{\frac{j2\pi m(nY-\tilde{n})}{YN}} + \hat{\eta}_{\tilde{n},v} \\ &= \begin{cases} \sqrt{Y}d_{n,v} + \hat{\eta}_{\tilde{n},v}, & \text{if } \tilde{n} = nY, \\ \hat{\eta}_{\tilde{n},v}, & \text{otherwise,} \end{cases} \end{aligned} \tag{30}$$

where

$$\hat{\eta}_{\tilde{n},v} = \frac{1}{\sqrt{YN}} \sum_{m=0}^{YN-1} \hat{\eta}_{m,v} e^{-\frac{j2\pi m\tilde{n}}{YN}}. \tag{31}$$

Finally, symbol recovery is achieved,

$$\hat{d}_{n,v} = \frac{\hat{\Theta}_{nY,v}}{\sqrt{Y}} = d_{n,v} + \frac{\hat{\eta}_{nY,v}}{\sqrt{Y}}, \tag{32}$$

where $v \in [1, Y - 1]$.

The proposed scheme demonstrates that it can resist interference from multipath effects using only one CP, and can utilize a single-tap equalizer for equalization. This approach greatly saves on CP overhead and spectrum resources.

3. Combination of SR-OFDM and MIMO

The OFDM is known for its ability to combat frequency-selective fading and mitigate inter-symbol interference, and it pairs seamlessly with MIMO’s spatial diversity and multiplexing capabilities. By leveraging multiple antennas at both the transmitter and the receiver, MIMO enhances spectral efficiency, improves link reliability, and increases data throughput rates [16]. Moreover, the combination of OFDM and MIMO enables robust performance in challenging environments, such as urban areas with high levels of multipath propagation. This synergy not only boosts the system capacity and coverage but also enhances the overall network performance, making it a compelling choice for next-generation wireless communication systems. Therefore, we extend the proposed SR-OFDM into MIMO in this section, with N_r receiving antennas and N_t transmitting antennas, as shown in Figure 3. $N_t = 2$ and $N_p = 2$ are taken in this paper for the sake of simplicity, and they can be easily extended into larger values.

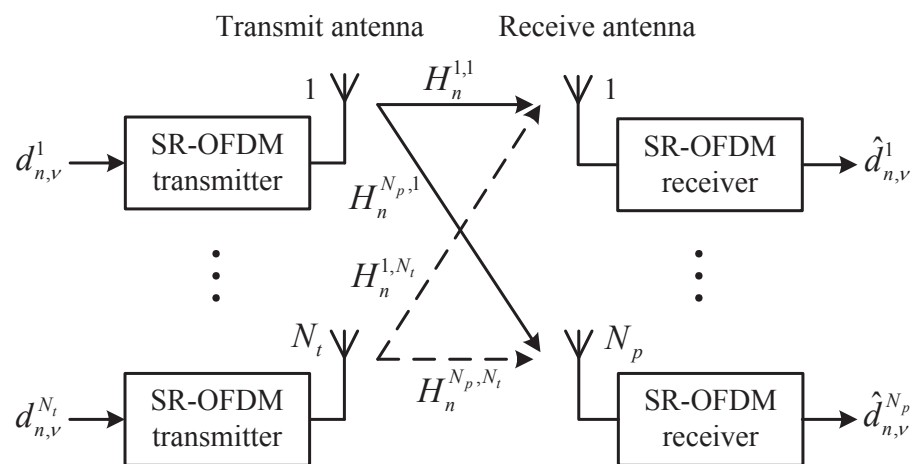


Figure 3. The diagram of the proposed combination of MIMO and SR-OFDM.

We denote that $d_{n,v}^t$ is transmitted via the t -th antenna at the transmitter. After passing through an IDFT transform, the signal is

$$s_v^t(k) = \frac{1}{\sqrt{N}} \sum_{n=0}^{N-1} d_{n,v}^t e^{j\frac{2\pi nk}{N}}, \quad k = 0, 1, \dots, N - 1. \tag{33}$$

Subsequently, the signal is constructed by Y rounds of repetition of $s_v^t(k)$, and for the p -th repetition, we multiply $s_v^t(k)$ by a phase coefficient $e^{j2\pi vp/Y}$, i.e.,

$$\tilde{s}_v^t(k) = s_v^t(k) e^{j\frac{2\pi vp}{Y}}. \tag{34}$$

Also, we note that $k = pN + \tilde{k}$, $p \in [0, Y - 1]$ and $\tilde{k} \in [0, N - 1]$.

After inserting the CP, the signal becomes

$$\tilde{s}_v^t(k) = \begin{cases} \tilde{s}_v^t(YN + k), & k = -L_{cp}, -L_{cp} + 1, \dots, -1, \\ \tilde{s}_v^t(k), & k = 0, 1, \dots, YN - 1. \end{cases} \tag{35}$$

Finally, we can obtain the transmitted signal, i.e.,

$$\tilde{s}^t(k) = \sum_{r=0}^{Y-1} \tilde{s}_v^t(k), \quad t \in [1, N_t]. \tag{36}$$

Let $h^{p,t}(k)$ be an MIMO channel, with the transmitting antenna index of t and receiving antenna index of p . After $\tilde{s}^t(k)$ passes through the channel, the signal of the p -th receiving antenna is

$$r^p(k) = \sum_{t=1}^{N_t} \tilde{s}^t(k) * h^{p,t}(k) + \eta^p(k), \tag{37}$$

where $\eta^p(k)$ is the AWGN noise at the p receiving antenna.

According to Equation (37), the received signal $r^p(k)$ is a linear combination of signals at different transmitting antennas, plus an AWGN noise. It is obvious that the demodulation of one receiving antenna will be the linear combination of demodulation of each transmitted signal. As a result, according to Equation (16), the demodulation is written as

$$y_{nY+v}^p = \sum_{t=1}^{N_t} \frac{H_{nY+v}^{p,t}}{N\sqrt{Y}} \sum_{n_0=0}^{N-1} d_{n_0,v}^t \sum_{k=0}^{YN-1} e^{j\frac{2\pi k(n_0-n)}{N}} e^{-j\frac{2\pi vk}{YN}} + \eta_{nY+v}^p, \tag{38}$$

where $H_n^{p,t}$ represents the frequency response of $h^{p,t}(k)$ with respect to the frequency index of n . η_{mR+r}^p is the noise, which is written as

$$\eta_{nY+v}^p = \frac{1}{\sqrt{YN}} \sum_{k=0}^{YN-1} \eta^p(k) e^{-j\frac{2\pi(nY+v)k}{YN}}. \tag{39}$$

For simplicity, we denote

$$x_{nY+v}^t = \frac{1}{N\sqrt{Y}} \sum_{n_0=0}^{N-1} d_{n_0,v}^t \sum_{k=0}^{YN-1} e^{j\frac{2\pi k(n_0-n)}{N}} e^{-j\frac{2\pi vk}{YN}}. \tag{40}$$

Next, (38) is rewritten as

$$y_{nY+v}^p = \sum_{t=1}^{N_t} H_{nY+v}^{p,t} x_{nY+v}^t + \eta_{nY+v}^p. \tag{41}$$

Subsequently, the matrix form of Equation (41) is obtained as

$$\begin{pmatrix} y_{nY+v}^1 \\ y_{nY+v}^2 \\ \vdots \\ y_{nY+v}^{N_p} \end{pmatrix} = \begin{pmatrix} H_{nY+v}^{1,1} & H_{nY+v}^{1,2} & \cdots & H_{nY+v}^{1,N_t} \\ H_{nY+v}^{2,1} & H_{nY+v}^{2,2} & \cdots & H_{nY+v}^{2,N_t} \\ \vdots & \vdots & \ddots & \vdots \\ H_{nY+v}^{N_p,1} & H_{nY+v}^{N_p,2} & \cdots & H_{nY+v}^{N_p,N_t} \end{pmatrix} \cdot \begin{pmatrix} x_{nY+v}^1 \\ x_{nY+v}^2 \\ \vdots \\ x_{nY+v}^{N_t} \end{pmatrix} + \begin{pmatrix} \eta_{nY+v}^1 \\ \eta_{nY+v}^2 \\ \vdots \\ \eta_{nY+v}^{N_p} \end{pmatrix}. \tag{42}$$

When the receiving antenna number is larger than the transmitting antenna number, based on Equation (42), x_{nY+v}^t can be estimated as

$$\begin{pmatrix} \hat{x}_{nY+v}^1 \\ \hat{x}_{nY+v}^2 \\ \vdots \\ \hat{x}_{nY+v}^{N_t} \end{pmatrix} = \begin{pmatrix} H_{nY+v}^{1,1} & H_{nY+v}^{1,2} & \cdots & H_{nY+v}^{1,N_t} \\ H_{nY+v}^{2,1} & H_{nY+v}^{2,2} & \cdots & H_{nY+v}^{2,N_t} \\ \vdots & \vdots & \ddots & \vdots \\ H_{nY+v}^{N_p,1} & H_{nY+v}^{N_p,2} & \cdots & H_{nY+v}^{N_p,N_t} \end{pmatrix}^{-1} \cdot \begin{pmatrix} y_{nY+v}^1 \\ y_{nY+v}^2 \\ \vdots \\ y_{nY+v}^{N_p} \end{pmatrix}. \tag{43}$$

Note that the channel matrix is supposed to be available to the receiver. According to Equation (43), the estimation of x_{nY+v}^t can be obtained. Furthermore, according to Equation (40), the transmitted symbol $d_{n,v}^t$ at the t -th transmitter antenna can be recovered. Then, as mentioned above, according to Equations (17)–(32), the transmitted symbol $d_{n,v}^t$ can be obtained for each $v \in [1, Y - 1]$, respectively.

4. Simulation Results

This section will verify the performance of the proposed system scheme using simulations. Simulations were conducted based on a proposed scheme system employing quadrature phase shift keying (QPSK) modulation in a multipath channel. The multipath channel model adopted the Stanford university interim (SUI) [17], with parameters shown in Table 1. According to the proposed scheme system, there are $v = 2$ symbol repetitions, the number of subcarriers is 2048, and the subcarrier spacing is 15,000 Hz. This is the same subcarrier spacing as the long-term evolution (LTE) standard, which is set at 15,000 Hz, resulting in one symbol duration of $T = \frac{1}{15000} s = 66.7 \mu s$. Furthermore, to match the extended CP length used in LTE, the CP is set to 0.25 T, i.e., the CP length is 512 samples. Since $v = 2$, the proposed program will repeat the symbol two times. In the interest of fairness, for each SR-OFDM symbol transmitted, the classical OFDM scheme transmits two symbols and inserts two CPs.

Table 1. Profiles of SUI channel models.

Channel	SUI-3	SUI-5
Sampling Frequency (MHz)	30.72	30.72
Number of Paths	3	3
Power Profile (in dB)	0, -5.0, -10.0	0, -5.0, -10.0
Delay Profile (μs)	0, 0.4, 0.9	0, 4, 10

Figure 4 shows the bit error rate(BER) comparison in the AWGN Channel. The BER represents the probability of one bit being demodulated incorrectly, while E_b/N_0 (dB) represents the power ratio of one bit to the noise it carries. By observing the curves of BER, we can determine the probability of bit errors occurring under different noise energy ratios. Thus, the performance of the scheme against noise and channel effects is investigated. In

the case of the same transmission power, the proposed SR-OFDM achieves a 3 dB gain due to symbol repetition transmission on two occasions, as expected. Since the proposed scheme transmits twice as many symbols as OFDM, the total transmission power of OFDM is only half of that stated in the proposed scheme. It can be observed that as the number of symbol repetitions increases, the performance gain in terms of error rate also increases. If the transmission power of OFDM is doubled, the performance will be the same as that of the proposed scheme.

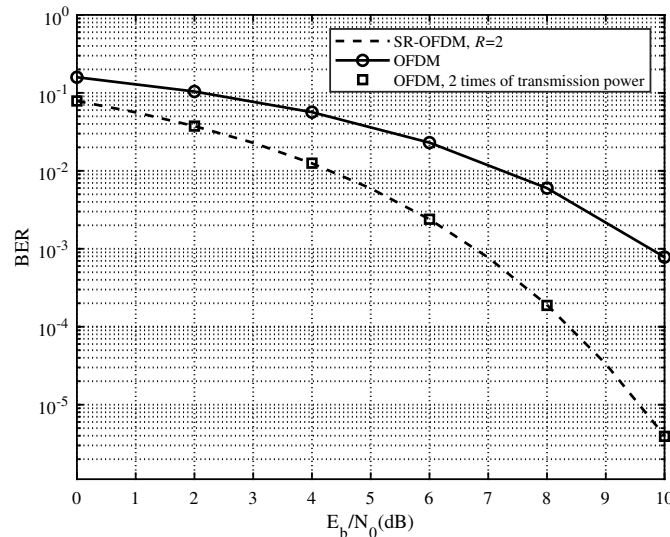


Figure 4. BER comparison in AWGN channel.

Figure 5 depicts the spectral efficiency comparison in the AWGN channel. The results indicate that the proposed scheme has better spectral efficiency. And the spectral efficiency of SR-OFDM will be better when the value of R is larger and the overhead of the CP is lower. As explained in Section 2.1, in the absence of CP overhead, one symbol $d_{m,r}$ is repeated R times, resulting in a time cost of RT . With the design of R branches, the SR-OFDM can deliver a total of RM data symbols within the time duration of RT (excluding CP overhead). Similarly, the classical OFDM can also deliver the same data symbols within RT (excluding CP overhead). Furthermore, there will be no difference in the transmission power for both schemes. However, when considering CP, the overhead for classical OFDM is $\frac{T_{cp}}{(T+T_{cp})}$, while the overhead for the proposed scheme is $\frac{T_{cp}}{(RT+T_{cp})}$, where T_{cp} represents the duration of the CP.

A comparison of the BER between SR-OFDM and OFDM in SUI-3 and SUI-5 channels is shown in Figures 6 and 7, respectively. The transmission power of classical OFDM is twice that of the proposed scheme. Compared to classical OFDM, the proposed SR-OFDM reduces CP overhead and saves time–frequency resources. To facilitate the comparison, we neglect the CP overhead to ensure that the total transmission power remains the same. Additionally, we assume that the channel estimation and timing synchronization will be perfect. In the AWGN channel, the error rate performance of both schemes is consistent. However, the delay of SUI-5 is greater than that of SUI-3. Both schemes perform similarly in both SUI-3 and SUI-5 channels. This implies that the proposed scheme can mitigate multipath effects without suffering from ISI. As shown in Equations (20) and (22), the proposed scheme can also be equalized by single-tap equalization, similar to the classical OFDM. Furthermore, the simulation results indicate that the receiver can separate the received signals corresponding to different $d_{m,r}$ relative to r , thereby reducing the demodulation complexity of SR-OFDM, as shown in Equation (16). Therefore, the proposed SR-OFDM significantly reduces the CP overhead and serves as an efficient multi-carrier waveform.

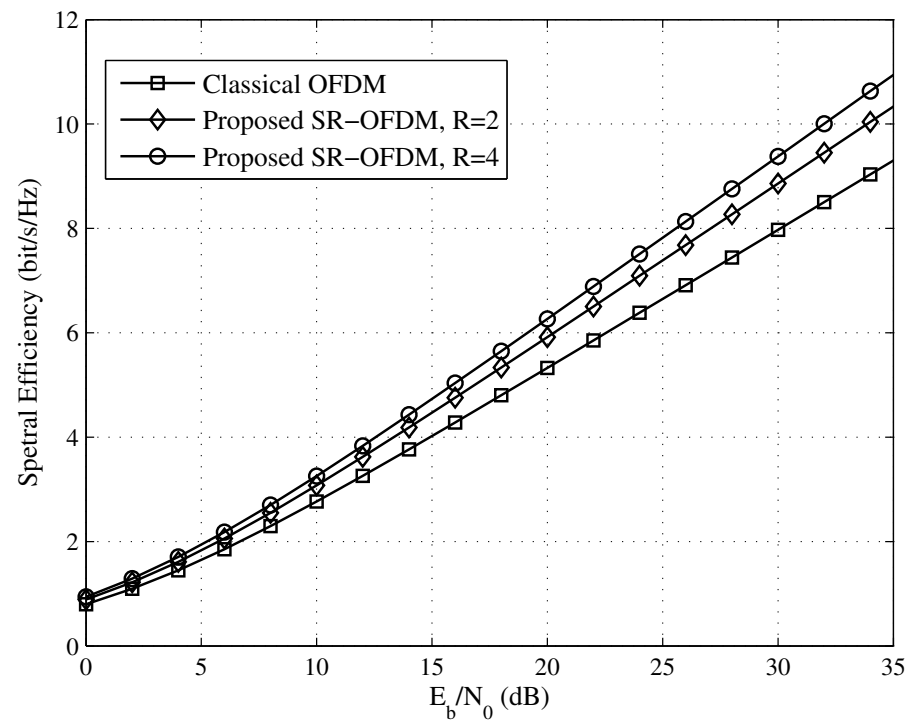


Figure 5. Spectral efficiency comparison in AWGN channel.

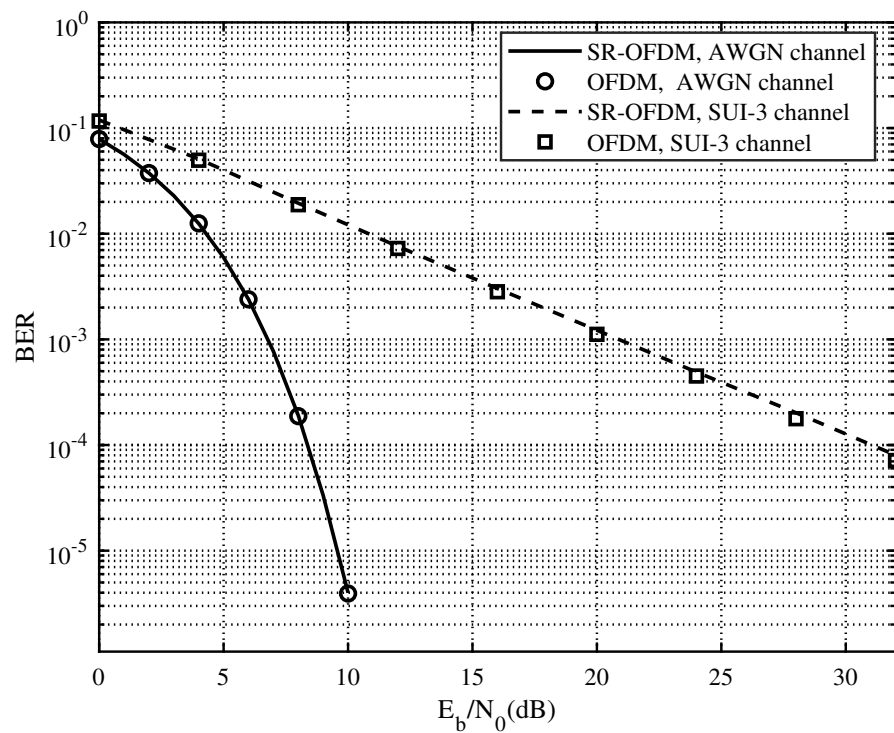


Figure 6. BER comparison for perfect channel estimation in SUI-3 and AWGN channels.

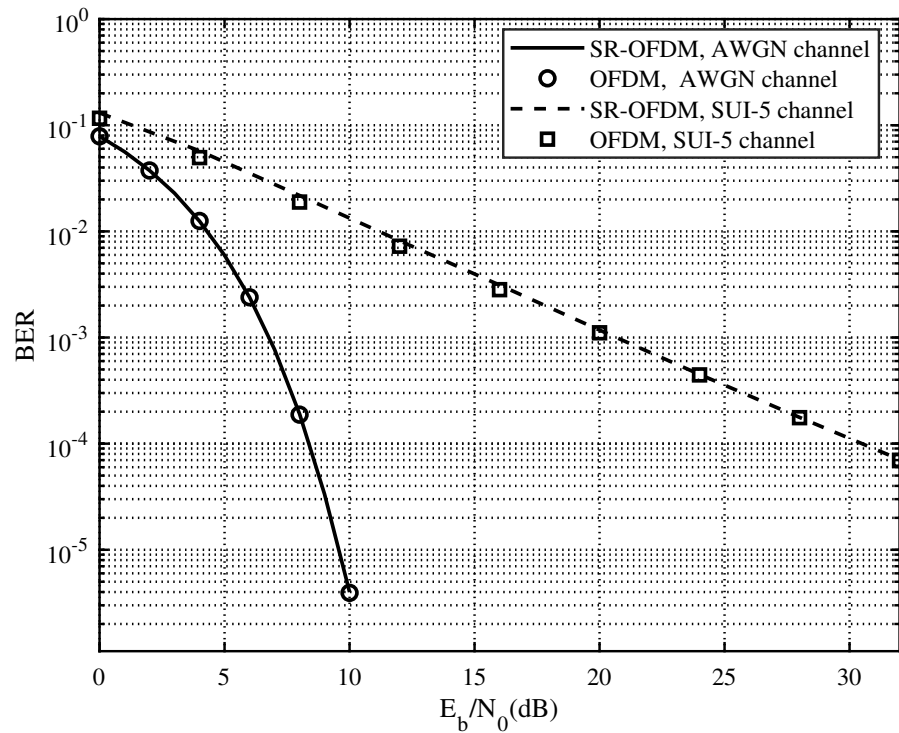


Figure 7. BER comparison for perfect channel estimation in SUI-5 and AWGN channels.

A comparison of BER based on MIMO is shown in Figure 8. Channel modeled as the SUI-5 channel. The antenna matrix for MIMO is 2×2 . The results indicate that both schemes have the same BER based on the MIMO technique.

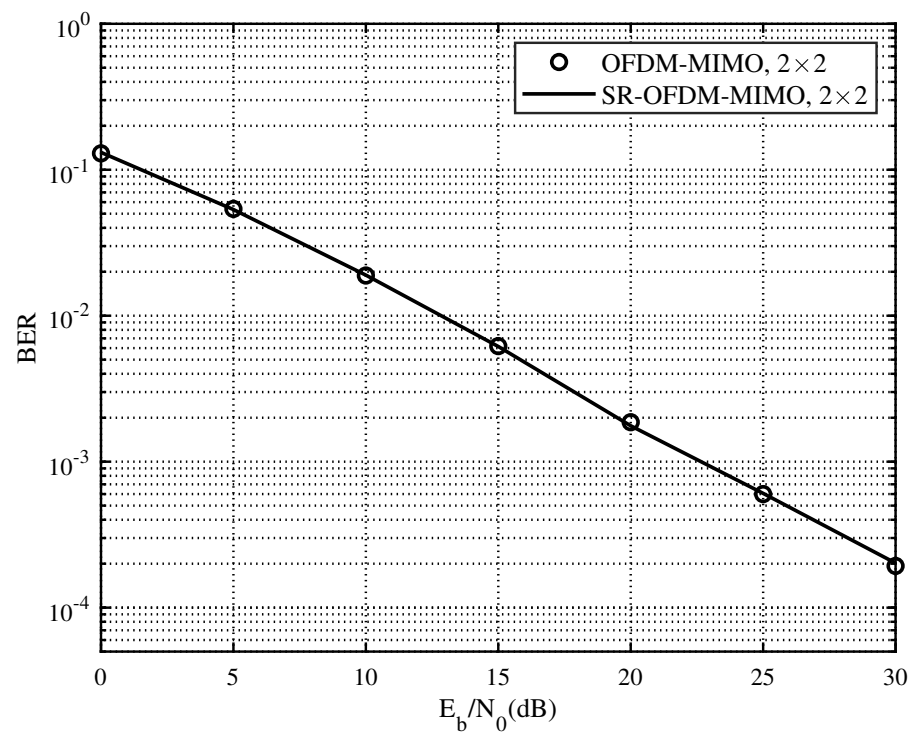


Figure 8. BER comparison based on 2×2 MIMO in SUI-5 channel.

To obtain a more general perspective of the proposed scheme for MIMO applications, we added a comparison of the BER in a 4×4 MIMO system in Figure 9. The channel was

modeled as the SUI-5 channel. The results show that both schemes have the same BER in 4×4 MIMO systems. Consequently, we conclude that combining SR-OFDM and MIMO does not introduce interference. It should be noted that the CSI is assumed to be a known entity and is typically obtained through channel estimation in practical applications. However, the channel estimation in SR-OFDM-MIMO is more challenging compared to conventional MIMO due to symbol overlap across multiple antennas. Therefore, the channel estimation in SR-OFDM-MIMO would be a meaningful research topic to investigate in the future.

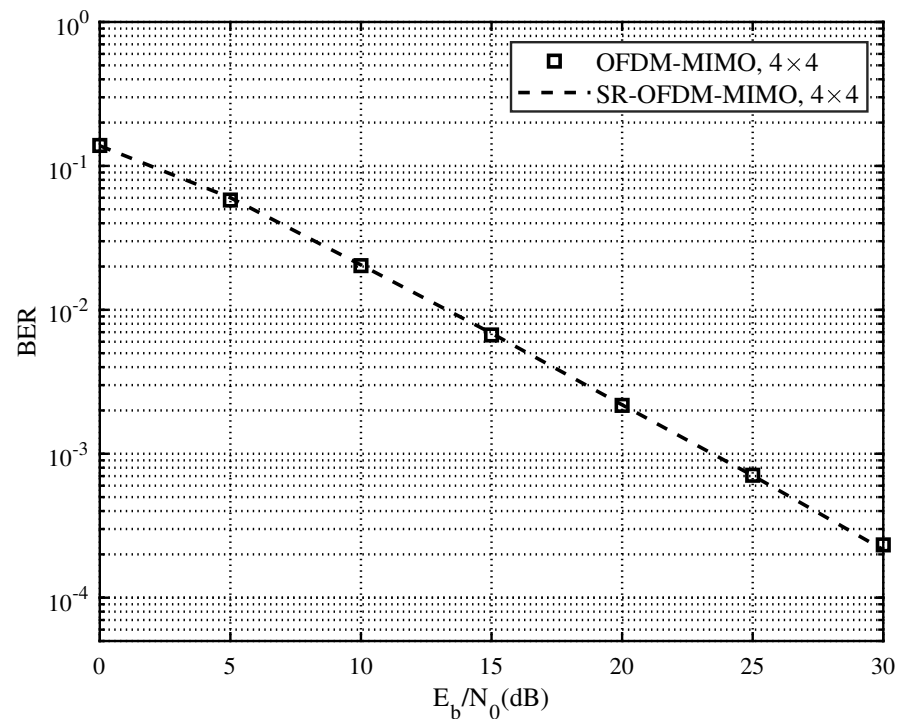


Figure 9. BER comparison based on 4×4 MIMO in SUI-5 channel.

5. Conclusions

In this paper, a low CP waveform SR-OFDM with symbol repetition is proposed. SR-OFDM significantly reduces the CP overhead but increases the complexity compared to classical OFDM. It is shown that a simple single-tap equalizer can effectively counteract the effects caused by multipath channels. In addition, we extend the proposed SR-OFDM to MIMO systems, and the results show that the proposed SR-OFDM combined with MIMO does not generate interference.

Author Contributions: Conceptualization, H.Y.; methodology, H.Y., J.L. and D.K.; formal analysis, H.Y.; investigation, H.Y., J.L. and D.K.; software, H.Y., B.W. and B.Z.; validation, H.Y., B.W. and S.L.; data curation, H.Y.; writing—original draft preparation, H.Y.; writing—review and editing, H.Y., J.L. and D.K.; supervision, J.L. All authors have read and agreed to the published version of the manuscript.

Funding: This work was financially supported in part by the Scientific Research Project of Education Department of Hubei Province with Grant numbers D20221702, Outstanding Young and middle-aged Scientific and Technological Innovation Team Project in Hubei Province with Grant numbers T2022059.

Data Availability Statement: The data used to support the findings of this study are available from the corresponding author upon request.

Conflicts of Interest: Author Baobing Wang was employed by the company Anhui Fengsung Electronics Co., Ltd. The remaining authors declare that the research was conducted in the absence of any commercial or financial relationships that could be construed as a potential conflict of interest.

References

1. Kong, D.; Xia, X.G.; Liu, P.; Zhu, Q. MMSE channel estimation for two-port demodulation reference signals in new radio. *arXiv* **2020**, arXiv:2007.14168.
2. Shen, Z.; Papasakellariou, A.; Montojo, J.; Gerstenberger, D.; Xu, F. Overview of 3GPP LTE-advanced carrier aggregation for 4G wireless communications. *IEEE Commun. Mag.* **2012**, *50*, 122–130. [[CrossRef](#)]
3. Gowda, N.M.; Sabharwal, A. CPLink: Interference-free reuse of cyclic-prefix intervals in OFDM-based networks. *IEEE Trans. Wirel. Commun.* **2018**, *18*, 665–679. [[CrossRef](#)]
4. Celebi, S. Interblock interference (IBI) minimizing time-domain equalizer (TEQ) for OFDM. *IEEE Signal Process. Lett.* **2003**, *10*, 232–234. [[CrossRef](#)]
5. Kim, N.; Shin, O.S.; Lee, K.B. Sum rate maximization with shortened cyclic prefix in a MIMO-OFDM system. *IEEE Trans. Veh. Technol.* **2018**, *67*, 12416–12420. [[CrossRef](#)]
6. Rong, J.; Liu, F.; Miao, Y. Integrated radar and communications waveform design based on multi-symbol OFDM. *Remote Sens.* **2022**, *14*, 4705. [[CrossRef](#)]
7. Soltani, N.; Cheng, H.; Belgiovine, M.; Li, Y.; Li, H.; Azari, B.; D’Oro, S.; Imbiriba, T.; Melodia, T.; Closas, P.; et al. Neural network-based OFDM receiver for resource constrained IoT devices. *IEEE Internet Things Mag.* **2022**, *5*, 158–164. [[CrossRef](#)]
8. Shi, W.; Zhao, C.; Jiang, M. Reduced complexity interference cancellation for OFDM systems with insufficient cyclic prefix. In Proceedings of the 2019 11th International Conference on Wireless Communications and Signal Processing (WCSP), Xi’an, China, 8 December 2019; pp. 1–6.
9. Liu, X.Q.; Chen, H.H.; Lyu, B.Y.; Meng, W.X. Symbol cyclic shift equalization PAM-OFDM—A low complexity CP-free OFDM scheme. *IEEE Trans. Veh. Technol.* **2016**, *66*, 5933–5946. [[CrossRef](#)]
10. Liu, X.; Chen, H.H.; Meng, W.; Lyu, B.Y. Successive multipath interference cancellation for CP-free OFDM systems. *IEEE Syst. J.* **2018**, *13*, 1125–1134. [[CrossRef](#)]
11. Xiao, Y.; Li, X.; Wei, P.; Xiao, L.; Xiang, W. Hybrid prefix OFDM transmission toward future wireless communications. *IEEE Access* **2018**, *6*, 22341–22352. [[CrossRef](#)]
12. Kong, D.; Liu, P.; Fu, Y.; Ding, J.; Quek, T.Q. Reduction of cyclic prefix overhead in narrow-band internet of things (nb-iot) systems. *IEEE Wirel. Commun. Lett.* **2020**, *10*, 517–521. [[CrossRef](#)]
13. Kong, D.; Qu, D.; Jiang, T. Time domain channel estimation for OQAM-OFDM systems: Algorithms and performance bounds. *IEEE Trans. Signal Process.* **2013**, *62*, 322–330. [[CrossRef](#)]
14. Kong, D.; Zheng, X.; Zhang, Y.; Jiang, T. Frame repetition: A solution to imaginary interference cancellation in FBMC/OQAM systems. *IEEE Trans. Signal Process.* **2020**, *68*, 1259–1273. [[CrossRef](#)]
15. Kong, D.; Li, J.; Luo, K.; Jiang, T. Reducing pilot overhead: Channel estimation with symbol repetition in MIMO-FBMC systems. *IEEE Trans. Commun.* **2020**, *68*, 7634–7646. [[CrossRef](#)]
16. Liu, P.; Jin, S.; Jiang, T.; Zhang, Q.; Matthaiou, M. Pilot power allocation through user grouping in multi-cell massive MIMO systems. *IEEE Trans. Commun.* **2016**, *65*, 1561–1574. [[CrossRef](#)]
17. Jain, R. Channel models: A tutorial. In *Proceedings of the WiMAX Forum AATG*; Washington University St. Louis, Department CSE: St. Louis, MO, USA, 2007; Volume 10, pp. 10–12.

Disclaimer/Publisher’s Note: The statements, opinions and data contained in all publications are solely those of the individual author(s) and contributor(s) and not of MDPI and/or the editor(s). MDPI and/or the editor(s) disclaim responsibility for any injury to people or property resulting from any ideas, methods, instructions or products referred to in the content.